Journal of Materials Chemistry A

Accepted Manuscript

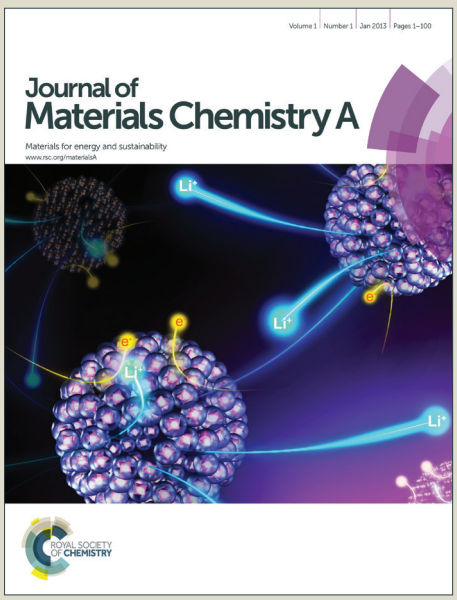

ROYAL SOCIETY OF CHEMISTRY

www.rsc.org/materialsA

Journal Name

RSCPublishing

ARTICLE

Size-controlled nitrogen-containing mesoporous carbon nanospheres by one-step aqueous self-assembly strategy†

Jia Wang,[a] Hongyang Liu,[a] Jiangyong Diao, [a] Xianmo Gu, [a] Haihua Wang,[a] Junfeng Rong,[b] Baoning Zong,[b] Dang Sheng Su*[a]

mesCite this: DOI: 10.1039/x0xx00000x

Received 00th January 2012, Accepted 00th January 2012

DOI: 10.1039/x0xx00000x

www.rsc.org/

Nitrogen-containing mesoporous carbon nanospheres with tunable sizes have been prepared through an aqueous self-assembly process with F127 as a template and morphological control agent, and 3-aminophenol as carbon and nitrogen sources. The sphere sizes could be simply tuned by optimizing the concentration of F127 and ammonia. Compared with a traditional nanocasting method and a hydrothermal process, the present one-step method has striking features of simply synthesis process and easy introduction of the nitrogen atom into the carbon nanospheres. The feasibility of the fabrication method may open up a new way to the synthesis of heteroatom-containing carbon nanospheres with mesoporous structure. The prepared nitrogen-containing mesoporous carbon nanospheres exhibits a good catalytic performance in the direct dehydrogenation of ethylbenzene due to its unique mesostructure and abundant oxygen and nitrogen functional groups.

Introduction

Mesoporous carbon with high surface areas, open mesostructure, and tailored frame-work compositions has attracted considerable attention.[1-3] They are used in a wide range of applications, such as catalysis[4-7], sensing[8], supercapacitors[9] and lithium-ion batteries[10]. So far, many efforts have been made to synthesize mesoporous carbon with well-controlled pore structure, composition and porosity.[11-14] Despite of these achievements, effectively control of morphology and internal mesostructure of mesoporous carbon still remains a challenge.

Nanocasting method is a common method to synthesize mesoporous carbon by employing nanosized mesoporous silica or silica spheres as a hard template.[15-19] However, this method is a low efficiency, high cost and fussy process. Moreover, the mesostructrue, pore size and morphology of the replicated mesoporous carbon are limited to the used silica template. Recently, organic-organic self-assembly method has been used to synthesize ordered mesoporous carbon (OMC) through either a "hydrothermal"[20-22] method or evaporation-induced self-assembly (EISA)[23, 24] process. Morphologies of the mesoporous carbon materials synthesized from the EISA process are usually films and monolithic that depends on the synthesis conditions,[14, 23] whereas the hydrothermal route could yield carbonaceous monoliths with hierarchical porosities[21, 22] or uneven spherical mesoporous carbon particles with the size from hundreds of nanometers to a few micrometers[20].

In the past few years, aerosol-assisted[25] and suspension assisted[26] self-assembly synthesis methods have been used to obtain mesoporous carbon spheres (MCS). More recently, ordered body-centered cubic mesoporous carbon nanoparticles with spherical morphology and uniform size were synthesized by a low-concentration hydrothermal route, which was developed by Fang and co-workers. [27] Likewise, Li *et al.* demonstrated a similar hydrothermal process to obtain spherical and rod-like OMC by changing the concentration of F127.[28] In these two processes, the key to the success is to control the concentration of F127 and well-separate the two processes of the micelle assembly and the polymer condensation. Another important factor is that they used phenol-formaldehyde (PF) oligomers as starting units. Therefore, these synthesis routes need multiple steps and a prolonged reaction process. Besides, some latest important contributions have also been developed by Qiao and co-workers to synthesize nitrogen-doped/undoped MCS *via* a step-by-step hydrothermal method with using the dual surfactants soft template in the aqueous-alcoholic solution.[29, 30] These processes extended the well-known Stöber method[31] to synthesize mesoporous carbon nanoparticles, and there are more tunable experimental parameters (such as the ratio of ethanol-water, the concentration of dual surfactants, and so on) to control the size and morphology of the carbon nanoparticles. Although this method is a great improvement for the synthesis of mesoporous carbon nanoparticles, it is still relatively complicated and requires multistep procedures (prepolymerization and hydrothermal solidification) resulting in

prolonged reaction process. Consequently, the development of facile and feasible methods to prepare mesoporous carbon nanoparticles is still necessary. Inspiringly, J. Tang *et al.*, obtained N-doped mesoporous carbon spheres with large mesopore sizes under milder conditions using the micelles of a high-molecular-weight block polymer PS-b-PEO as a template *via* a facile micelle route,[32] which has more advantage over step-by-step hydrothermal strategy in the aspect of obtaining large pore and simple synthesis route.

The aqueous self-assembly is an interesting route and has been used to synthesize OMC.[12, 33-35] Compared with the nonaqueous EISA pathway, the aqueous route shows better reproducibility and unlimited fabrication batch size. Unfortunately, to our best knowledge, only a few reports focused on the morphology control of mesoporous carbon by this aqueous self-assembly route,[36,37] because it is difficult to control micelle assembly and polymer condensation in one-pot aqueous synthesis process. In order to well-separate micelle assembly and polymer condensation, hexamine was used as a slow release source of formaldehyde (HCHO) and thus to control the kinetics off the polymerization reaction.[35]

Nitrogen atom is usually induced into the carbon matrix, resulting in the improvement of surface polarity, electron donor properties of the carbon matrix, and introducing active basic/catalytic sites on the carbon surface.[38] In our previous work, we found that it is feasible to synthesize nitrogen-containing ordered mesoporous carbon using 3-aminophenol as carbon and nitrogen sources in one-pot aqueous self-assembly process.[39] Such progress in the synthesis strategy encourages us to explore a more simple method to directly synthesize nitrogen-containing mesoporous carbon spheres in one-pot aqueous self-assembly process.

In the present work, we report a facile aqueous self-assembly strategy for the synthesis of the nitrogen-containing mesoporous carbon nanospheres (denoted as NMCS) with tunable sizes. In this process, F127 is not only a soft template forming the mesostructure, but also a morphological control agent, which is a novel feature in this work. Besides, similar to the synthesis of silica spheres[31], carbon spheres[40,41], ammonia is also used to catalyze the polymerization of 3-aminophenol and HCHO, and control the spherical morphology and sizes. Compared with previous reports[27-30], the current synthesis is carried out under milder conditions (compared with hydrothermal conditions) in one-pot aqueous process and has simpler synthesis process. The NMCS with high specific surface areas (~600 m^2 g^{-1}) and large pore volume (~0.57 cm^3 g^{-1}) are obtained by the pyrolysis of spherical nitrogen-containing resols-F127 composites at 600 °C under Ar atmosphere. The size of NMCS ranges from 90 to 220 nm by varying the concentration of F127 and/or ammonia. Due to its high thermal stability, even after carbonized at 800 °C, the NMCS still maintains spherical morphology except for smaller size (164 nm) compared with NMCS carbonized at 600 °C. This method may provide a simple and feasible strategy for the preparation of heteroatom-containing carbon nanoparticles to some extent by designing appropriate synthesis process. The potential application of NMCS in the dehydrogenation of ethylbenzene was also demonstrated.

Experiment

Materials and preparation

Poly(ethylene oxide) - block - poly(propylene oxide)- block - poly (ethylene oxide) triblock copolymer Pluronic F127 ($PEO_{106}PPO_{70}PEO_{106}$, M_W=12,600) was purchased from Sigma-Aldrich Corp. 3-aminophenol (MAP) were purchased from Alfa Aesar. Other chemicals were purchased from Sinopharm Chemical Reagent Corp. All chemicals were used as received without further purification.

Fig. 1 schematically illustrates the one-step aqueous process used for the synthesis of the NMCS. The detailed synthesis parameters are shown in Table S1. In a typical procedure, F127 was dissolved in the deionized water to form spherical micelle solution. After the addition of 3-aminophenol (MAP), hexamine (HMT) and 28 wt% aqueous ammonia, the resulting mixed solution was stirred at the room temperature for 1 h to obtain homogeneous micellar solution. Then the solution was poured into a flask and transferred into an oil bath equipped with a water-cooled condenser at 80 °C stirred for 24 h. The as-made product (spherical nitrogen-containing resols-F127 composites, denoted as APS) was collected by sedimentation separation, washed with water and ethanol and dried at 40 °C for 12 h. Carbonization was carried out in a tubular furnace under an inert atmosphere with the heating rate of 1 ℃ min^{-1} at 350 °C for 1 h and then heating at 600 °C or 800 °C for 3 h. The final sample was denoted as NMCS-x-T (x represents the corresponding synthesis parameters, as shown in Table S1, and T represents the carbonization temperature).

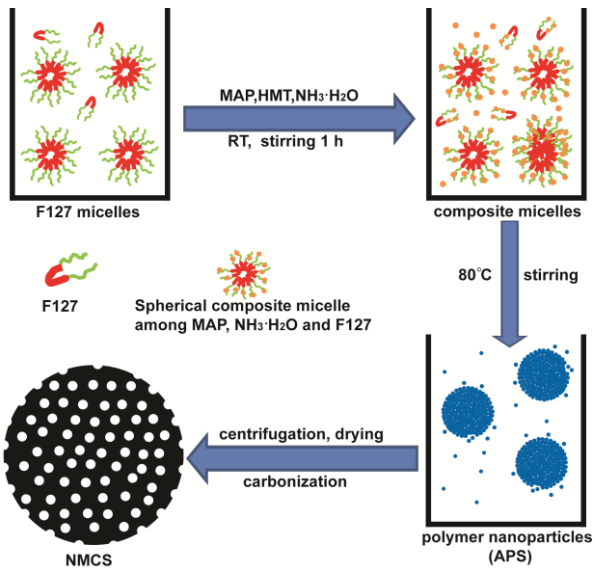

Fig. 1 Schematic illustration of the formation of NMCS.

Measurement of catalytic performance

Direct dehydrogenation of ethylbenzene was carried out at 550 ℃ for 14 h in a fixed bed flow microreactor. A catalyst of 100 mg was placed at the center of the reactor using quartz wool plugs. After the system was heated to 550 ℃ and kept for 10 min in He atmosphere, the reactant of 2.8 % ethylbenzene with feed flow rate 10 mL min^{-1} and He as balance was then

fed into the reactor from a saturator kept at 38.9 ℃. Quantitive analysis of the collected reaction products (ethylbenzene, styrene, toluene, and benzene) was performed on an Agilent 7890 GC equipped with HP-5 and DB-wax capillary column connected to FID and a CarboPlot capillary column connected to TCD.

Characterization

Small-angle XRD patterns were recorded on a Rigaku D/Max-2500PC diffractometer with a Cu Kα radiation operating at 50 kV, 300 mA. The mesostructure and morphology of the NMCS was characterized by a FEI T12 transmission electron microscopy (TEM) with an accelerating voltage of 120 kV. Scanning electron microscopy (SEM) images were taken using an FEI Nano450 scanning electron microscope operated at 10-15 kV and the sphere size was measured over 100 particles from SEM micrographs. Nitrogen adsorption-desorption data were measured with a Micromeritics ASAP 3020 analyser at 77 K. Prior to the measurements, the samples were degassed at 120 ℃ for 12 h. The specific surface areas were calculated by the Brunauer-Emmett-Teller (BET) method using adsorption data in a relative pressure range from 0.02 to 0.20. The total pore volumes (V_t) were estimated on the basis of the adsorbed amount at a relative pressure of 0.985. The pore size distributions (PSD) was calculated from adsorption data of isotherms using the Barett-Joyner-Halenda (BJH) model. Surface chemistry of the samples was investigated using an ESCALAB 250 instrument with Al Kα X-rays (1486.6 eV). The elemental composition of C, N, O, and H was measured on a TCH-600 Hydrogen/Nitrogen/Oxygen Analyzer. Raman spectra of samples on SiO_2/Si were performed with a Labram HR800 spectrometer and a He/Ne laser at 633 nm (50× objective) was selected as the excitation source.

Results and discussion

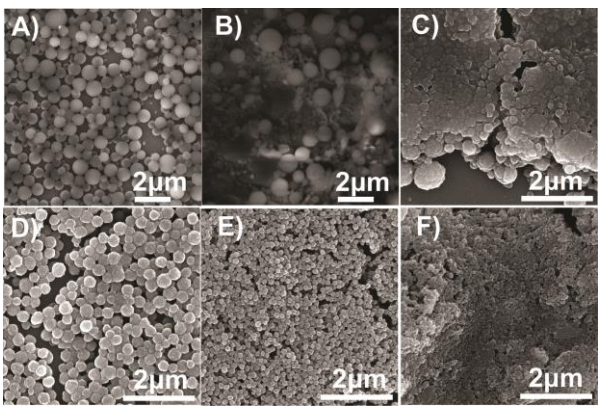

Fig. 2 SEM images of APS synthesized at different concentration of F127: A) 0 B) 1.5 C) 3.8 D）4.6 E) 5.3 F) 6.1 mM. 3-Aminophenol, 10 mmol; HMT, 5 mmol; ammonia concentrations: 0.37 M. The magnification is 20000× in Fig. B and 40000× in other Figures.

In the soft-template method of making ordered mesoporous carbon (OMC), a key step is to form micelles through self-assembly of amphiphilic block copolymer (such as F127, P123) which is used as a structure-direct agent for the synthesis of OMC. And the formation of ordered mesostructrue (space group, $P6mm$, $Im\bar{3}m$, $Ia\bar{3}d$) is affected by the concentration of amphiphilic block copolymer.[11, 13] Recent study also pointed out that the morphology of the micelles plays an important role in determining the morphology of the final product of OMC.[28] Unfortunately, a very limited number of open literatures involve the morphology control using F127 as structure-direct agent and morphology control agent in one-pot aqueous process. In our experiment, spherical mesoporous carbon is observed in the comparatively high concentration of F127 which is different from the result reported by Fang.[27] In order to rationalize the influence of different parameters on the formation of APS, the effects of the concentration of F127 and ammonia are investigated systematically. Fig. 2 shows SEM images of APS synthesized with different concentration of F127 while fixing the other experimental parameters (Table S1). In the absence of F127 (Fig. 2A), the collected sample (APS-1) presents the morphology of the dispersed microspheres with a smooth surface and a broad size distributions from hundreds of nanometers to a few micrometers. The formation of these spheres may be attributed to the nucleation of the aromatic clusters driven by surface tension.[42] After adding 1.5 mM F127 (Fig. 2B, APS-2), a small number of uneven spherical particles could be formed on the polymer base, suggesting that F127 affects the nucleation and growth of the aromatic clusters. Although some larger blocks are only formed, the blocks are comprised of many uneven spherical particles when continue raising the concentration of F127 to 3.8 mM (Fig. 2C, APS-3). These results indicate that F127 has a positive effect on the formation of spherical nanoparticles but it is not enough to promote the uniform spheres under low F127 concentration. As shown in Fig. 2D and E (APS-4 and APS-5), with the concentration of F127 ranging from 4.5 to 5.3 mM, uniform spheres are obtained, and the sphere size decreases from 324±45 to 136±14 nm (Table S1). When F127 concentration increases to 6.1 mM, smaller APS nanoparticles are achieved, but the aggregation of nanoparticles is very serious (Fig. 2F, APS-6). In addition, the APS yield is found to be very sensitive to the concentration of F127. Fig. S1 plots the dependence of the yield of APS and NMCS versus the concentration of F127 and ammonia. When F127 concentration is raised from 4.6 to 5.3 mM under 0.37 M ammonia, the yield of APS would decrease from 48 % to 21 % (Fig. S1A). We propose that higher F127 concentration may lead to the partial assembly among F127 and some resols-F127 composite micelles are too small to complete the rearrangement, resulting in the lower yield of APS synthesized at higher F127 concentration, as shown dark brown upper solution after centrifugation (Fig. S2). To sum up, it is believed that F127 facilitates the formation of spheres and its concentration plays a very important role in forming uniform spheres and controlling the size. The process involves in the assembly of MAP and spherical F127 micelles to form spherical resols-F127 composites through hydrogen-bond and then rearrangement of these composites driven by polymerization between MAP and HCHO produced by hydrolysis of HMT at 80 °C (Fig. 1).

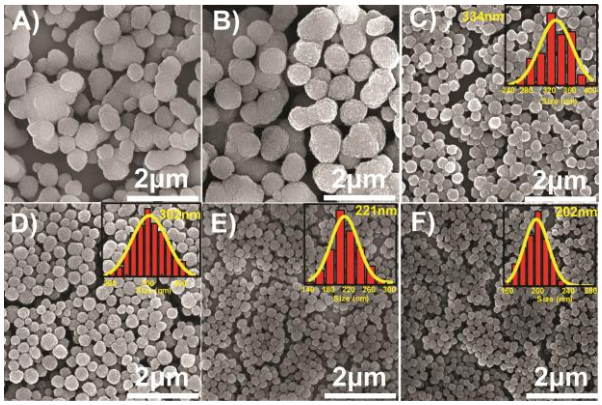

Fig. 3 SEM images of APS synthesized by using different ammonia concentration: A) 0 B) 0.14 C) 0.37 D) 0.57 E) 0.71 F) 0.86 M. 3-Aminophenol, 10 mmol; HMT, 5 mmol; F127 concentration: 4.6 mM. The magnification is 40000×.

In the typical synthesis process of silica spheres, such as Stöber method[31], ammonia was usually used as a morphological catalyst causing the formation of spherical silica particles. Therefore, we investigate whether it has an effect on the morphology of the particles. As shown in Fig. 3A, in the absence of ammonia, the produced sample (APS-7) has irregular spherical morphology and uneven size. Although ammonia could be produced through the hydrolysis of HMT, obviously it is not enough to regulate the spherical morphology even if the concentration of ammonia is raised to 0.14 M (Fig. 3B, APS-8). As shown in Fig. 3C-F, uniform spheres are achieved when continue to raise the ammonia concentration (APS-4, APS-9, APS-10 and APS-11). The size of APS decreases with the increase of ammonia concentration. For example, the size ranges from 324±45 (APS-4) to 202±16 nm (APS-11) with raising ammonia concentration from 0.37 to 0.86 M (Table S1). The increase of ammonia concentration may accelerate the polymerization and facilitate the formation of more nuclei, and thus decrease the sizes of spheres.[40] Moreover, NH_4^+ could adhere to the outer surface of spheres and prevent the spheres aggregation, resulting in smaller nanoparticles.[41] In addition, we also observe that the APS yield is dependent on the concentration of ammonia, and it decreases from 58 % to 28 % with the increase of ammonia concentration from 0 to 0.86 M under 4.6 mM F127 (Fig. S1B). The main reason is still unknown, but we propose that the reason may be lower amount of formaldehyde converted from HMT in high ammonia concentration because the hydrolysis of HMT could be restrained. Unfortunately, no precipitation could be obtained after the solution was heated at 80 °C for 24 h if HMT was replaced by stoichiometric formaldehyde and ammonium hydroxide. Similar phenomenon was also observed in the previous reporter.[35] The detailed mechanism is yet not clear, but these results clearly indicate that HMT cannot be replaced simply by formaldehyde. In order to further understand the phenomenon of the decreasing yield of APS with increasing ammonia concentration, we investigated the effect of the HMT amount. Interestingly, if we raise the amount of HMT, the APS yield would increase (Fig. S1C). This result may elucidate that the lower formaldehyde amount may result in the lower yield of APS in high ammonia concentration to some extent, because raising HMT amount could increase its hydrolysis extent.

Like phenol-formaldehyde resols, aminophenol - formaldehyde resols are also of interest because of the high yield of carbon conversion during the carbonization.[40] Nitrogen-containing mesoporous carbon nanospheres could be obtained by the pyrolysis of spherical nitrogen-containing resols-F127 composites at 600 or 800 ℃ under Ar atmosphere. The carbonization yield is about 60 % regardless of the variation of F127 or ammonia concentration (Fig. S1). SEM image of APS-4 (Fig. S3A**)** shows that APS-4 has uniform spherical morphology and rough surfaces, but no pores are observed through the particles (Fig. S3B). As shown in Fig. 4A, NMCS-4-600, obtained by the pyrolysis of the APS-4 at 600 ℃, has a spherical morphology with rough surface. Moreover, obviously mesopore system could be observed on these spheres through TEM (Fig. 4C), which is attributed to the removal of F127 after calcination. The sphere size decreases from 324±45 nm of APS-4 to 225±23 nm of NMCS-4-600 (Table S2), which may be ascribed to the further solidification of resols. Due to its high thermal stability, the spherical morphology is maintained and there exists obvious mesostructure through these particles after carbonized at 800 ℃ (Fig. 4B and D), except for further decrease of the sphere size to 164±23 nm (Table S2).

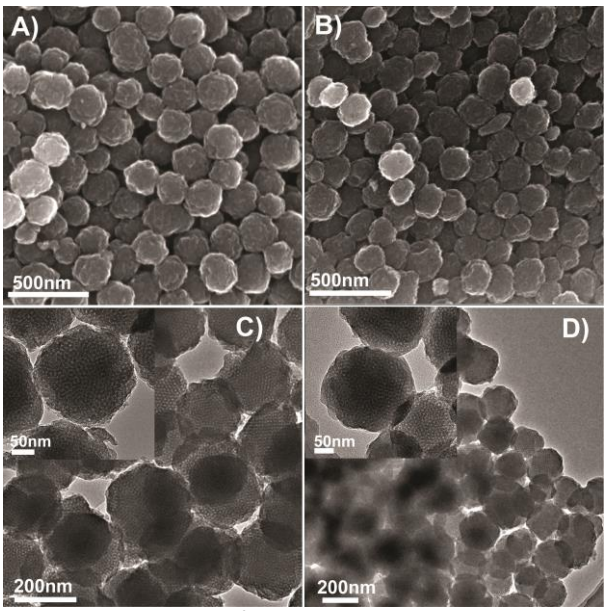

Fig. 4 SEM and TEM images of NMCS-4-600 (A and C) and NMCS-4-800 (B and D). The insets in (C) and (D) are respective high-magnification TEM images.

Typical N_2 adsorption-desorption isotherms and corresponding pore size distributions of the APS-4, NMCS-4-600, and NMCS-4-800 are shown in Fig. 5 A and B. A clear hysteresis loop in the P/P_0=0.35~0.6 range is observed for NMCS-4-600 and NMCS-4-800, suggesting a uniform mesopore. Besides, at a higher relative pressure (P/P_0>0.95), the N_2 adsorption amount obviously increases, indicating multi-layer adsorption on the out surfaces of nanoparticles. According to Brunauer-Emmett-Teller method, the specific surface areas (S_{BET}) is calculated to be 497 m^2 g^{-1} of NMCS-4-600 and 793 m^2 g^{-1} of NMCS-4-800. The total pore volumes are 0.36 cm^3 g^{-1} of

NMCS-4-600 and 0.54 cm^3 g^{-1} of NMCS-4-800 (Table S2). However, for APS-4, except for the clear adsorption at P/P_0>0.95, the adsorption amount is very low and the S_{BET} is only about 9 m^2 g^{-1}. So, the removal of F127 after calcination results in formation of mesostructure which contributes to the increase of specific surface areas and pore volumes. Moreover, if no F127 is added, namely for NMCS-1-600, no mesoporous structure is observed through the particles even after calcination at 600 ℃ (Fig. S4). Its specific surface areas is about 403 m^2 g^{-1}, which mainly originates from micropore because of no mesostructure existing. The small-angle XRD is a good tool to characterize the order of the mesostructure. Fig. S5 shows the small-angle XRD patterns of the typical NMCS samples synthesized at different conditions. The small-angle XRD patterns of NMCS-4-600, NMCS-5-600, NMCS-7-600, and NMCS-11-600 shows two resolved peaks at 2θ =0.5-2, suggesting that ordered mesostructure could be obtained at adequate concentration range of F127 and/or ammonia. The d-spacing value ratio of the two peaks is about 1:1/$\sqrt{3}$, which could be indexed as the (110) and (211) reflections of a body-centered cubic mesostructrue ($Im\bar{3}m$). However, there is no signal in the small-angle XRD pattern of NMCS-1-600 (Fig. S5A), indicating no ordered mesoporous structure, which is the same with the results of TEM (Fig. S4). Besides, the ordered mesostructure is still maintained after carbonized at 800 ℃ (Fig. S5C). Typical SEM, TEM images, and N_2 adsorption-desorption isotherms of other NMCS synthesized at different conditions by changing the concentration of F127 or ammonia are shown in Fig. S6. All these results indicate that NMCS with various sizes (from 97 nm to 220 nm, Table S2) could be obtained by the pyrolysis of APS, whose size could be tuned by changing the concentration of F127 and ammonia. The pore size of these samples is about 4.0-4.7 nm (Table S2), suggesting that the pore size mainly depends on the surfactant F127. In previous reports about the synthesis of ordered mesoporous carbon,[34,35] small hydrocarbons (such as hexadecane, decane or 1,3,5-trimethylbenzene) could be used as a swelling agent to change the mesoporous structure or enlarge the pore size. Here, if we added aliquots of 1,3,5-trimethylbenzene (denoted as TMB) in the synthesis process (Table S1 and S2, NMCS-12-600), irregular nanoparticles with the size of ~100 nm were obtained and the pore size increased to 5.1 nm compared with NMCS-4-600, indicating that TMB could enlarge pore size and reduce the particle size (Fig. S7). However, no signals could be observed in the small-angle XRD pattern of NMCS-12-600 (Fig. S5D) indicating disordered mesostructure. Although the exact mechanism of the morphology change after adding TMB molecules is still unclear, we propose that it may be related to the decrease of hydrophilic/hydrophobic volume ratios of F127. In general, the smaller sphere size results in larger specific surface areas (unit: m^2 g^{-1}). However, we observe that the specific surface areas increases with the decrease of the sphere size except for NMCS-9-600. Similar results were also found in the previous report.[27] We propose that there are two main factors: the sphere size and mesopore amount on each sphere. The smaller sphere results in less pore amount. Contrarily, the smaller sphere size contributes to higher specific surface areas. Therefore, the conjunct effects of these two factors may result in this phenomenon. Of course, we could not exclude the effects of the inhomogeneity.

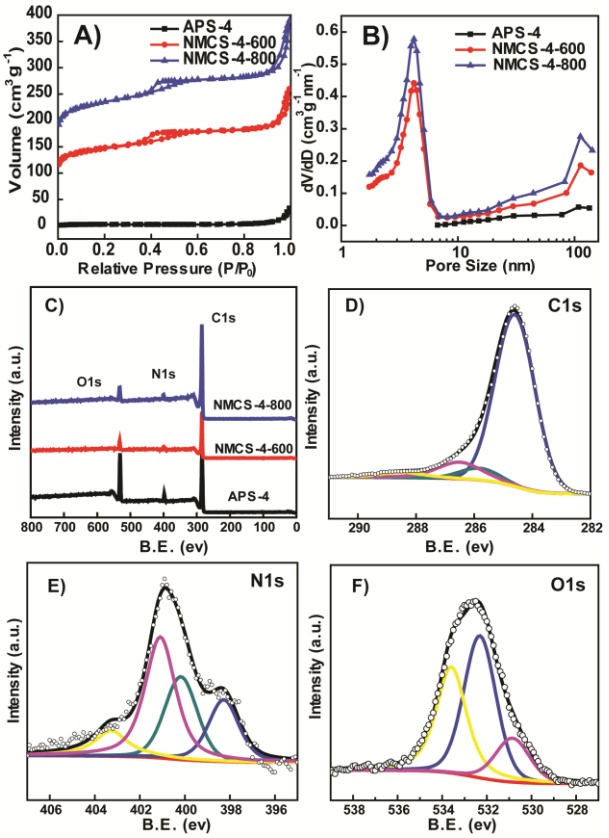

Fig. 5 N_2 adsorption-desorption isotherms (A) and corresponding pore size distributions (B) of APS-4, NMCS-4-600 and NMCS-4-800. XPS spectra of APS-4, NMCS-4-600 and NMCS-4-800 (C) and the C1s spectrum (D), N1s spectrum (E) and O1s spectrum (F) of NMCS-4-800.

In order to understand these samples' composition, elemental analysis was conducted (Table S3). Elemental analysis reveals that APS-4 consists of C (65.9 wt%), N (3.8 wt%), H (7.3 wt%), and O (23 wt%). These values indicate that the framework is a kind of polymer. The composition of this framework changes to C/N/H/O of 100/8.9/2.3/11.4 when the material is heated at 600 °C. This phenomenon suggests that the polymer framework transforms to carbon, accompanied with the removal of small molecules. Besides, the incorporation of N in the framework can be maintained even after high temperature carbonization. Additionally, NMCS-1-600 and NMCS-4-600 have similar elemental composition, suggesting that the composition is mainly depended on the carbonization temperature. XPS spectra were employed to detect the surface chemistry of the fabricated APS-4, NMCS-4-600, and NMCS-4-800. Fig. 5C shows XPS spectra of APS-4, NMCS-4-600, and NMCS-4-800. Clear signals from C, N, O of these three samples are observed, suggesting that N could be introduced into the resols-F127 composites *via* polymerization of MAP and HCHO, which is consistent with our previous results.[39] The presence of O species arises from precursors and lots of O species loss during the pyrolysis resulting in 7.4 at% O content of NMCS-4-600 and 5.7 at% O content of NMCS-4-800 (Table S3). The N content also decreases with the increase of the carbonization temperature due to decomposition and conversion of nitrogen functional groups. For example, the N content decreases from 5.1 at% to 3.1 at% after carbonized at 800 ℃. These changes are consistent with the

elemental analysis results (Table S3). The spectrum of C1s of the NMCS-4-800 (Fig. 5D) could be deconvoluted into four single peaks that correspond to C=C (284.5±0.1 eV), C-N or C-C (285.8±0.2 eV), C-O (286.5±0.1 eV), and C=N/C=O (288.5±0.1 eV) functional groups.[38] The N1s spectrum (Fig. 5E) are fitted into four peaks with binding energies of 398.2±0.2, 400.1±0.2, 401.1±0.2 and 403.1±0.2 eV that correspond to pyridinic-N, pyrrolic-N, graphitic-N and oxidized-N, respectively.[43-45] The spectrum of O1s of the NMCS-4-800 (Fig. 5F) could be deconvoluted into three single peaks with binding energies of 530.9±0.3 eV, 532.7±0.2 eV, and 533.8±0.1 eV that correspond to quinone, C=O, and C-OH, respectively.[9] The quinone and C=O functional groups are the most possible active sites for the C-H activation of light hydrocarbon or ethylbenzene due to their substantial electron density at the oxygen.[46] Therefore, the nitrogen-containing mesoporous carbon nanospheres with abundant surface functional groups may be applied into the dehydrogenation of ethylbenzene. Besides, the shape and position of C1s, N1s and O1s of NMCS-4-600 (Fig. S8) are similar to those of NMCS-1-600 suggesting that the nature and coordination of C, N, O in NMCS are mainly depended on the carbonization temperature. As a result, specific surface areas, pore volumes, and N types and content are mainly affected by the calcination temperature according to above discussion.

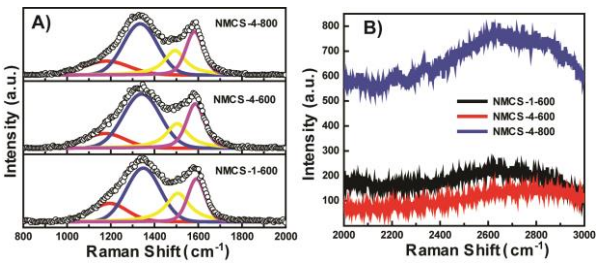

Fig. 6 The first-order for Raman spectra and corresponding curve fits (A) and second-order Raman spectra (B) of the NMCS-1-600, NMCS-4-600 and NMCS-4-800 using a He-Ne laser (λ =633nm).

Raman scattering spectrum is an excellent probe for studying the microstructure of carbon materials.[47] It has been claimed that the first-order Raman lines relate to structural order within the carbon sheets whereas the second-order Raman lines relate to the stacking disorder along the crystallographic c-aixs. [48] Therefore, in the first-order Raman spectra, the intensity, line width of D band and behaviour of I_D/I_G ratio are sensitive to the defects and graphitic extent. As shown in Fig. 6A, all these samples exhibit four main feature bands in the 800-2000 cm^{-1} region: the disordered graphitic lattice (~1200 cm^{-1}), the defect-related D-band (1335±5 cm^{-1}), the amorphous carbon (such as pentagon and heptagon) structure A-band (1490±10 cm^{-1}), and the ideal graphite lattice G-band (1595±5 cm^{-1}). Table S4 shows the corresponding fitting parameters. The broad peak of D-band (FWHM: 185±10 cm^{-1}) indicates a glassy carbon framework, [11] which is consistent with the results of high I_D/I_G ratio of NMCS-1-600 and NMCS-4-600 (2.18 and 2.08, respectively). The I_D/I_G ratio of NMCS-4-800 is about 1.98 which is slightly lower than that of NMCS-1-600 and NMCS-4-600, suggesting that it is difficult to obtain higher graphitic extent for the produced NMCS except that it is carbonized at very high temperature. [11, 49] The big I_D/I_G of the Raman peaks is an indicator of more defects or amorphous carbon on graphitic carbon materials.[50] Such defects may be saturated by oxygen atoms to produce more oxygen functional groups (Fig. 5C). Moreover, broad peak in the range of 2400-3000 cm^{-1} is observed in the second-order Raman spectra (Fig. 6B), which may be attributed to the associated overtone of D band (also named as 2D band) corresponding to small crystallite sizes and the presence of high proportions of edge planes in their structures.[51]

Based on the above observation and previous works performed by other groups[27-30, 32-34, 39], the possible formation process of the nitrogen-containing mesoporous carbon nanospheres is proposed as shown in Fig. 1. It is believed that the micelles morphology is affected by the concentration of F127. When the F127 concentration is above 4.6 mM, spherical F127 micelles are formed first in the aqueous solution. After adding MAP, HMT and ammonia water, spherical composite micelles are formed under the driving of hydrogen-bond interaction among F127, MAP, H_2O, and NH_3. During the stirring process at 80 ^oC, the spherical composite micelles could be solidified to the nitrogen-containing resols-F127 composites through cross-linking between MAP and HCHO which is produced by the hydrolysis of HMT. Simultaneously, the cross-linking also drives the small spherical micelles to accumulate and rearrange. As a result, a large spherical nitrogen-containing resols-F127 composites with partially ordered cubic mesostructure is formed. The removal of F127 after carbonization leaves behind the open and accessible mesopore array through the spheres. It is proposed that the morphology of the solidified composite polymer particles is determined by their respective original micelle morphology.[28] With the increase of F127 concentration, the smaller spherical micelles could be formed, thus resulting in the decrease of APS sizes. However, the increase of F127 concentration also results in excessive cross-linking between micelles which may lead to low yield of APS and serious aggregation among resols-F127 composites. Besides, the concentration of ammonia also plays important roles in controlling the morphology and size under adequate F127 concentration, which is similar with the results of previous reports.[40, 41] The appropriate concentration range of F127 (4.6-5.3 mM) and ammonia (0.37-0.85 M) are necessary to achieve comparatively uniform nanoparticles.

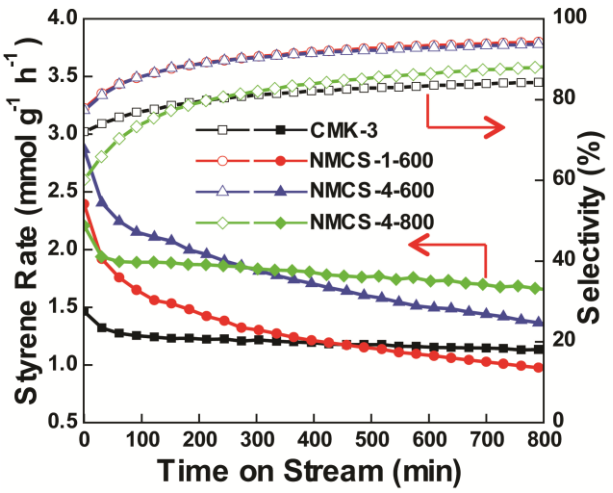

Fig. 7 Catalytic performance of NMCS-1-600, NMCS-4-600, NMCS-4-800, and CMK-3 for direct dehydrogenation of ethylbenzene to styrene. Reaction conditions: 550 ^oC, 2.8 % of Ethylbenzene in He, 10 mL min^{-1}, 100 mg catalyst.

The high specific surface areas, open pore system, and abundant surface functional groups make nitrogen-containing porous carbon promising materials as a metal-free catalyst. [52] The introduction of nitrogen atom into carbon matrix can increase the electron density of carbon materials and therefore strengthen the basicity and weaken the acidity of the catalyst, which may result in an improvement in catalytic activity for dehydrogenation of propane or ethylbenzene.[53-55] The catalytic performance of the developed NMCS and CMK-3 (synthesized using SBA-15 and sucrose as a template and a carbon source, respectively, following the reported procedure.[56]) was examined (Fig. 7). All the developed NMCS series catalysts have a better initial styrene rate than CMK-3, although CMK-3 has the highest specific surface areas, which indicates that N may play an important role in this reaction. Nitrogen-containing CMK-3 (denoted as N-CMK-3, Tables S3) was also tested as a catalyst for this reaction. As shown in Fig. S9, the styrene rate and selectivity of N-CMK-3 are all enhanced compared with CMK-3 after introducing the nitrogen into the CMK-3, also suggesting the important role of nitrogen. The quinone and C=O functional groups are the most possible active sites for the C-H activation which has been confirmed.[46] The introduction of a nitrogen atom into a carbon matrix can increase the electron density of carbon materials and therefore strengthen the basicity of the catalyst, which may result in an improvement in catalytic activity for styrene production.[53] Compared with NMCS-1-600, NMCS-4-600 exhibits a better styrene rate (1.2 mmol g^{-1} h^{-1} vs 0.8 mmol g^{-1} h^{-1}) and they have similar styrene selectivity (95 %) at 14 hours, ascribed to the easy accessibility of the catalytic active sites (C=O and quinone) in NMCS-4-600 for the ethylbenzene molecules, because the two materials have approximate specific surface areas, O content, and N content except that NMCS-4-600 has open mesostructure. As shown in the Fig. 7 and Fig. S9, NMCS-4-800 exhibits the best conversion of ethylbenzene and stability. The styrene selectivity (90 %) on the NMCS-4-800 is slightly lower than NMCS-4-600 (95 %) and higher than CMK-3 (85 %). After reaction, obvious changes are observed on the surface texture (Fig. S10). The specific surface areas obvious decreases and the mesostructure is not conspicuous, especially for NMCS-4-600 and NMCS-1-600 according to the N_2 adsorption-desorption results of catalysts after reaction. However, clear mesostructure could still be observed from TEM images (Fig. S11), indicating that the decrease of specific surface areas is mainly attributed to the block of micropore due to coke. Small-angle XRD patterns of the NMCS-4-600 and NMCS-4-800 catalysts after reaction (Fig. S11D) shows two small peaks confirming that ordered mesostructure is still maintained, which is the same with the TEM results. Similar result was also obtained in the previous reports[5-7]. Naturally, the microstructure of the NMCS is similar to activated carbon showing a disordered long-range ordering carbon atoms. Activated carbon is also active in the DH of propane to propene, but deactivates rapidly until very low activity is exhibited.[7] Therefore, the open mesostructure overmatches micropore system, due to its advantage for mass transport and good thermal stability.[5] Besides, XPS results after reaction (Table S5) indicate that nitrogen and oxygen content decrease in all these samples, but the decrease content of NMCS-4-800 is lower than NMCS-4-600, which may be one of reasons for the higher performance of NMCS-4-800 than NMCS-4-600. According to the results of Raman spectra after reaction (Table S4 and Fig. S12**)**, the increase of I_D/I_G ratio of all these samples indicates the production of coke on the surface, especially in the micropore sites. The low decrease extent for the NMCS-4-800 (0.05, Table S5) also suggests its higher resistance for coke.

Conclusions

In summary, we demonstrate a facile aqueous approach for the synthesis of the nitrogen-containing mesoporous carbon nanospheres (NMCS) with comparatively uniform and tunable size. The highlight in this synthesis is the utilization of F127 to control the spherical morphology, and at the same time to be as a template forming the mesostructure. Compared with the synthesis of the mesoporous carbon spheres using a nanocasting method or a hydrothermal route in the previous reports, our approach is convenient and time-short, which may open up a new way to the fabrication of heteroatom-containing carbon nanospheres with mesoporous structure.

- ✧ Firstly, we find that F127 is not only a soft template forming the mesostructure, but also a morphological control agent in this aqueous process.
- ✧ Secondly, the size of NMCS could be regulated by varying the concentration of F127 and/or ammonia. The addition of 1,3,5-trimethylbenzene could enlarge the mesopore size, but result in smaller nanoparticles with irregularly morphology.
- ✧ At last, NMCS with open mesostructure and abundant oxygen and nitrogen functional groups shows a better catalytic performance than that of nitrogen-containing bulk carbon spheres without mesostructure and CMK-3 for directly dehydrogenation of ethylbenzene. However, the improvement of the catalytic performance of NMCS is still indispensible especially for the catalytic stability in order to realize its real application in the catalysis, although the stability is improved after calcination at 800 ^{o}C.

Acknowledgements

This work was supported by the National Natural Science Foundation of China (21203214, 21133010, 51221264, 21261160487), MOST (2011CBA00504), "Strategic Priority Research Program" of the Chinese Academy of Sciences (Grant No. XDA09030103), the China Postdoctoral Science Foundation (2012M520652). Dr. Zhenhua Sun, Mr Yangming Lin, Mr Rui Huang and Mr. Shuchang Wu are gratefully acknowledged for his stimulating discussions.

Notes and references

[a]*Shenyang National Laboratory for Materials Science, Institute of Metal Research, Chinese Academy of Sciences, 72 Wenhua road, Shenyang 110016, P. R. China.*
Email: dangsheng@fhi-berlin.mpg.de, dssu@imr.ac.cn
[b]*Research Institute of Petroleum Processing, 18 Xueyuan Road, Haidian District, Beijing,100083, PR China.*
†Electronic Supplementary Information (ESI) available: additional figures. See DOI: 10.1039/c000000x/

1 T. Y. Ma, L. Liu and Z. Y. Yuan, *Chem. Soc. Rev.*, 2013, **42**, 3977.
2 C. D. Liang, Z. J. Li and S. Dai, *Angew. Chem. Int. Ed.*, 2008, **47**, 3696.
3 J. Lee, J. Kim and T. Hyeon, *Adv. Mater.*, 2006, **18**, 2073.
4 S. H. Joo, S. J. Choi, I. Oh, J. Kwak, Z. Liu, O. Terasaki and R. Ryoo, *Nature*, 2001, **412**, 169.
5 D. S. Su, J. J. Delgado, X. Liu, D. Wang, R. Schlogl, L. F. Wang, Z. Zhang, Z. C. Shan and F. S. Xiao, *Chem. Asian. J.*, 2009, **4**, 1108.
6 L. Liu, Q. F. Deng, B. Agula, X. Zhao, T. Z. Ren and Z. Y. Yuan, *Chem. Commun.*, 2011, **47**, 8334.
7 L. Liu, Q. F. Deng, B. Agula, T. Z. Ren, Y. P. Liu, B. Zhaorigetu and Z. Y. Yuan, *Catalysis Today*, 2012, **186**, 35.
8 D. Lee, J. Lee, J. Kim, H. B. Na, B. Kim, C. H. Shin, J. H. Kwak, A. Dohnalkova, J. W. Grate, T. Hyeon and H. S. Kim, *Adv. Mater.*, 2005, **17**, 2828.
9 X. C. Zhao, Q. Zhang, B. S. Zhang, C. M. Chen, A. Q. Wang, T. Zhang and D. S. Su, *J. Mater. Chem.*, 2012, **22**, 4963.
10 H. S. Zhou, S. M. Zhu, M. Hibino, I. Honma and M. Ichihara, *Adv. Mater.*, 2003, **15**, 2017.
11 Y. Meng, D. Gu, F. Q. Zhang, Y. F. Shi, L. Cheng, D. Feng, Z. X. Wu, Z. X. Chen, Y. Wan, A. Stein and D. Y. Zhao, *Chem. Mater.*, 2006, **18**, 4447.
12 A. H. Lu, B. Spliethoff and F. Schüth, *Chem. Mater.*, 2008, **20**, 5314.
13 Y. Wan, X. F. Qian, N. Q. Jia, Z. Y. Wang, H. X. Li and D. Y. Zhao, *Chem. Mater.*, 2008, **20**, 1012.
14 Y. Meng, D. Gu, F. Q. Zhang, Y. F. Shi, H. F. Yang, Z. Li, C. Z. Yu, B. Tu and D. Y. Zhao, *Angew. Chem. Int. Ed.*, 2005, **44**, 7053.
15 Z. Lei, N. Christov, L. L. Zhang and X. S. Zhao, *J. Mater. Chem.*, 2011, **21**, 2274.
16 M. Wallau, L. Dimitrov and E. A. Urquieta-Gonz áfez, *Studies in Surface Science and Catalysis*, 2005, **156**, 535.
17 Y. D. Xia and R. Mokaya, *Adv. Mater.*, 2004, **16**, 886.
18 Y. D. Xia, Z. X. Yang and R. Mokaya, *Chem. Mater.*, 2006, **18**, 140.
19 C. Z. Yu, J. Fan, B. Z. Tian, D. Y. Zhao and G. D. Stucky, *Adv. Mater.*, 2002, **14**, 1742.
20 D. Liu, J. H. Lei, L. P. Guo and K. J. Deng, *Carbon*, 2011, **49**, 2113.
21 L. Liu, F. Y. Wang, G. S. Shao and Z. Y. Yuan, *Carbon*, 2010, **48**, 2089.
22 Y. Huang, H. Q. Cai, D. Feng, D. Gu, Y. H. Deng, B. Tu, H. T. Wang, P. A. Webley and D. Y. Zhao, *Chem. Commun.*, 2008, 2641.
23 C. F. Xue, B. Tu and D. Y. Zhao, *Adv. Funct. Mater.*, 2008, **18**, 3914.
24 M. Florent, C. F. Xue, D. Y. Zhao and D. Goldfarb, *Chem. Mater.*, 2012, **24**, 383.
25 Y. Yan, F. Q. Zhang, Y. Meng, B. Tu and D. Y. Zhao, *Chem. Commun.*, 2007, 2867.
26 D. H. Long, F. Lu, R. Zhang, W. M. Qiao, L. Zhan, X. Y. Liang and L. C. Ling, *Chem. Commun.*, 2008, 2647.
27 Y. Fang, D. Gu, Y. Zou, Z. X. Wu, F. Y. Li, R. C. Che, Y. H. Deng, B. Tu and D. Y. Zhao, *Angew. Chem. Int. Ed.*, 2010, **49**, 7987.
28 M. Li and J. Xue, *Journal of colloid and interface science*, 2012, **377**, 169.
29 J. Liu, T. Y. Yang, D. W. Wang, G. Q. (Max) Lu, D. Y. Zhao and S. Z. Qiao, *Nat. Commun.*, 2013, **4**, 2798.
30 T. Y. Yang, J. Liu, R. F. Zhou, Z. G. Chen, H. Y. Xu, S. Z. Qiao and M. J. Monteiro, *J. Mater. Chem. A.*, 2014, **2**, 18139.
31 W. Stöber and A. Fink, *Journal of colloid and interface science*, 1968, **26**, 62.
32 J. Tang, J. Liu, C. L. Li, Y. Q. Li, M. O. Tade, S. Dai, and Y. Yamauchi, *Angew. Chem. Int. Ed.*, 2014, DOI: 10.1002/anie.201407629
33 F. Q. Zhang, Y. Meng, D. Gu, Y. Yan, C. Z. Yu, B. Tu and D. Y. Zhao, *J. Am. Chem. Soc.*, 2005, **127**, 13508.
34 F. Q. Zhang, Y. Meng, D. Gu, Y. Yan, Z. X. Chen, B. Tu and D. Y. Zhao, *Chem. Mater.*, 2006, **18**, 5279.
35 D. Liu, J. H. Lei, L. P. Guo, D. Qu, Y. Li and B. L. Su, *Carbon*, 2012, **50**, 476.
36 F. Q. Zhang, D. Gu, T. Yu, F. Zhang, S. H. Xie, L. J. Zhang, Y. H. Deng, Y. Wan, B. Tu and D. Y. Zhao, *J. Am. Chem. Soc.*, 2007, **129**, 7746.
37 D. Gu, H. Bongard, Y. Meng, K. Miyasaka, O. Terasaki, F. Q. Zhang, Y. H. Deng, Z. X. Wu, D. Feng, Y. Fang, B. Tu, F. Schüth and D. Y. Zhao, *Chem. Mater.*, 2010, **22**, 4828.
38 Z. X. Wu, P. A. Webley and D. Y. Zhao, *J. Mater. Chem.*, 2012, **22**, 11379.
39 J. Wang, H. Y. Liu, X. M. Gu, H. H. Wang and D. S. Su, *Chem. Commun.*, 2014, **50**, 9182.
40 J. M. Zhao, W. X. Niu, L. Zhang, H. R. Cai, M. Y. Han, Y. L. Yuan, S. Majeed, S. Anjum and G. B. Xu, *Macromolecules*, 2013, **46**, 140.
41 J. Liu, S. Z. Qiao, H. Liu, J. Chen, A. Orpe, D. Y. Zhao and G. Q. (Max) Lu, *Angew. Chem. Int. Ed.*, 2011, **50**, 5947.
42 X. M. Sun and Y. D. Li, *Angew. Chem. Int. Ed.*, 2004, **43**, 597.
43 X. Q. Wang, C. G. Liu, D. Neff, P. F. Fulvio, R. T. Mayes, A. Zhamu, Q. Fang, G. R. Chen, H. M. Meyer, B. Z. Jang and S. Dai, *J. Mater. Chem. A.*, 2013, **1**, 7920.
44 R. Arrigo, M. Havecker, R. Schlogl and D. S. Su, *Chem. Commun.*, 2008, 4891.
45 S. Kundu, W. Xia, W. Busser, M. Becker, D. A. Schmidt, M. Havenith and M. Muhler, *Phys. Chem. Chem. Phys.*, 2010, **12**, 4351.
46 (a) J. Zhang, D. S. Su, R. Blume, R. Schlogl, R. Wang, X. G. Yang and A. Gajović, *Angew. Chem. Int. Ed.*, 2010, ***49***, *8640;* (b) R. Wang, X. Y. Sun, B. S. Zhang, X. Y. Sun, and D. S. Su, *Chem. Eur. J.*, 2014, **20**, 6324.
47 M. S. Dresselhausa, G. Dresselhausb, R. Saitoc and A. Jorio, *Physics Reports*, 2005, **409**, 47.
48 D. S. Knight and W. B. White, *J. Mater. Res.*, 1989, **4**, 385.
49 X. Q. Wang, C. D. Liang and S. Dai, *Langmuir*, 2008, **24**, 7500.
50 W. Qi, W. Liu, B. S. Zhang, X. M. Gu, X. L. Guo, and D. S. Su, *Angew. Chem. Int. Ed.*, 2013, **52**, 14224.
51 R. Silva, J. A. Sharab, and T. Asefa, *Angew. Chem. Int. Ed.*, 2012, **51**, 7171.
52 W. Z. Shen and W. B. Fan, *J. Mater. Chem. A.*, 2013, **1**, 999.
53 Z. K. Zhao, Y. T. Dai, J. H. Lin, G. R. Wang, *Chem. Mater.*, 2014, **26**, 3151.
54 C. L. Chen, J. Zhang, B. S. Zhang, C. L. Yu, F. Peng and D. S. Su, *Chem. Commun.*, 2013, **49**, 8151.
55 Z. K. Zhao, Y. T. Dai, *J. Mater. Chem. A.*, 2014, **2**, 13442.
56 S. Jun, S. H. Joo, R. Ryoo, M. Kruk, M. Jaroniec, Z. Liu, T. Ohsuna O. Terasaki, *J. Am. Chem. Soc.*, 2000, **122**, 10712.

Table of Contents

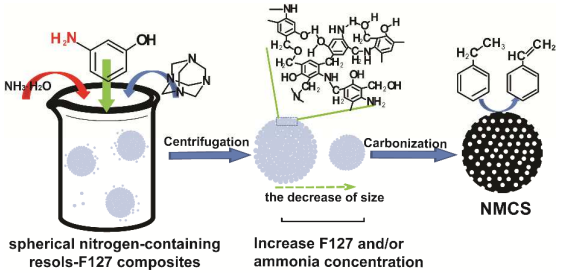

Nitrogen-containing mesoporous carbon nanospheres with tunable sizes have been prepared through an aqueous self-assembly process with F127 as a template and morphological control agent, and 3-aminophenol as carbon and nitrogen sources.